Meteoritics & Planetary Science 41, Nr 10, 1633–1646 (2006)
Abstract available online at http://meteoritics.org

Modification of impact craters in the northern plains of Mars: Implications for Amazonian climate history

M. A. KRESLAVSKY[1, 2*] and J. W. HEAD[1]

[1]Department of Geological Sciences, Brown University, Box 1846, Providence, Rhode Island, 02912, USA
[2]Astronomical Institute, Kharkov National University, Sumska 22, Kharkov, 61022, Ukraine
[*]Corresponding author. E-mail: kreslavsky@brown.edu

(Received 15 October 2005; revision accepted 10 April 2006)

Abstract–We measured the depth, wall steepness, and ejecta roughness and surveyed the wall and floor morphology of all craters 10–25 km in diameter within the typical Vastitas Borealis Formation in the northern lowlands of Mars north of 52°N. Two of the 130 craters have unusually rough ejecta; they are deep, have steep walls, and are apparently the youngest in the population. Icy mantles filling the local subkilometer-scale topographic lows is the main contribution to ejecta smoothing, which occurs at a time scale on the order of tens of Myr. Wall degradation and crater shallowing generally occur at longer time scales, comparable to the duration of the Amazonian period. Many craters are shallow due to filling of the crater with specific ice-rich material of uncertain origin. We use our collected data to infer the nature of the past climate back through the Amazonian, a period prior to ~10–20 Myr ago, when orbital parameter solutions are chaotic and one must rely on geological data to infer climate conditions. We conclude that moderately high obliquity and wide obliquity variations were probable during the last 40–160 Myr. We tentatively conclude that high obliquity peaks (>40–45°) may have occurred episodically through the last 210–430 Myr. A sharp step in the frequency distribution of wall steepness at 20° may indicate a geologically long period prior to that time where obliquity never exceeded 40–45°.

INTRODUCTION

The climate of Mars changes with time. Numerous traces of these changes have been identified in the geological record; a spectacular recent example is extinct glaciers in the equatorial region (e.g., Head et al. 2005). Among the forces causing climate change, the best understood and in some sense the most powerful is so-called "astronomical forcing," the change of spin and orbit parameters. These parameters define the insolation pattern on the planet and through it they control the entire climate system (e.g., see the review by Kieffer and Zent 1992). Among these parameters, the obliquity of the spin axis has long been recognized as the most powerful climate driver. For the Amazonian epoch, the latest three billion years of the Martian geological record, the climate change history to a first order is the history of obliquity variations, except, probably, for geologically short periods resulting from large impacts and major volcanic and water outflow events.

Obliquity oscillates with a period of ~125 kyr (Fig. 1). The amplitude of these oscillations is modulated with a period of ~1.3 Myr. The maximum oscillation amplitude is ~20°. In addition to these quasiperiodic oscillations, chaotic changes of mean obliquity occur at time scales of ~5 Myr and greater (Laskar and Robutel 1993). Due to the dynamically chaotic nature of these oscillations, predictive calculations of the spin/orbital parameters are possible only back to ~10–20 Myr before the present. Such calculations (e.g., Laskar et al. 2004) show that the oscillations around ~25° obliquity of the present epoch were preceded by a period of generally higher obliquity (~35 ± 10°) prior to about 5 Myr ago (Fig. 1).

Laskar et al. (2004) performed an extensive series of calculations of spin/orbital parameters for time spans much longer than 20 Myr. Although these calculations are not predictive, they provide a picture of probable obliquity variation patterns. The average obliquity over a large number of 250 Myr long calculations is ~35°. This mean value must not be considered an estimate of the actual mean obliquity for the last 250 Myr, because the mean obliquity varies widely from run to run. It is quite possible, however, that the typical obliquity in the recent geological past was higher than now. The calculations leave open the possibility of continuous variations of the mean obliquity at the 5 Myr time scale, of long duration of high or low mean obliquity, and so on.

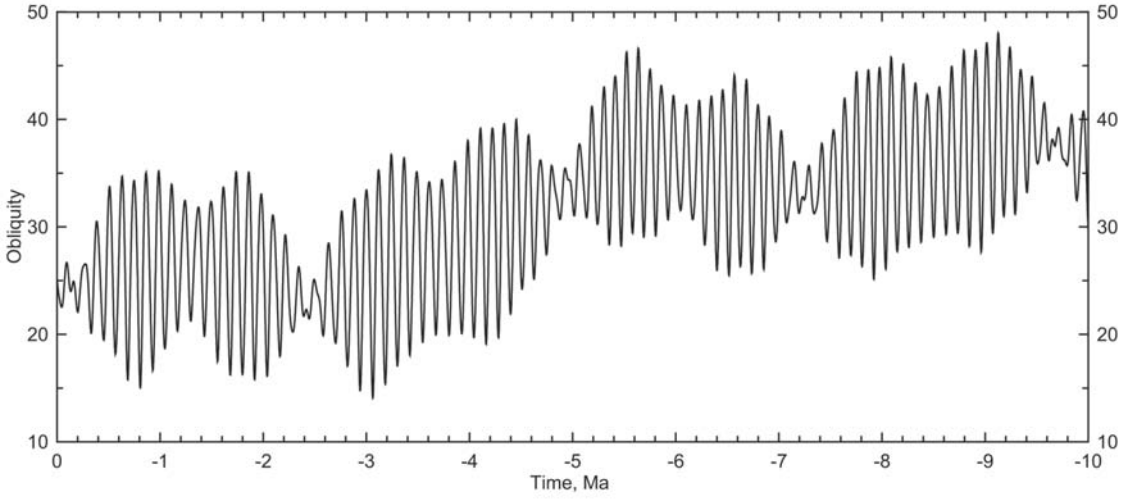

Fig. 1. Evolution of the spin axis obliquity of Mars for the last 10 Myr calculated by Laskar et al. (2004).

Since the calculations are not predictive, the nature of climate and climate-controlling obliquity in the geological past should be searched for in the geological record. In this analysis, we approach this problem by studying the modification of impact craters in the northern lowlands of Mars, and specifically those within the typical Vastitas Borealis Formation (e.g., Tanaka et al. 2003; Head et al. 2002; Kreslavsky and Head 2002b). This is the largest geological unit on Mars. It is thought to have a rather uniform age approximately at the Hesperian/Amazonian boundary and an accumulation population of relatively large impact craters (Tanaka et al. 2005). These craters were presumably formed in a rather similar environment and hence initially had similar morphologies. Their formation age is thought to be uniformly distributed through the Amazonian period. Figures 2a–2c show examples of the craters studied (referred to hereafter as craters A, B, and C). Crater A has a well-expressed, crisp ejecta sculpture with sharp morphological features, while crater B ejecta, having a generally similar morphology, is obviously much more subdued (compare Figs. 2a and 2b). These two craters clearly represent different stages of ejecta modification; crater A, characterized by much fresher ejecta morphology, is younger than crater B. We systematically studied the morphology and morphometry of the whole crater population to infer information about crater-alteration processes and their rates through the Amazonian period. Since the majority of candidate surface processes that may be responsible for crater alteration and degradation are related to surface-atmosphere interaction, the crater data set potentially contains constraints on the climate history in the Amazonian. Here we present some initial results of our analysis and their implications for climate history.

We first describe our observations, and then analyze the data set to assess the major processes of crater modification and to infer some basic conclusions about the nature, driving forces, and time scales of these processes. Finally, we consider some possible constraints on the obliquity history of Mars.

SURVEY

Crater Selection

We studied craters in the northern plains, and specifically those within typical areas of the Vastitas Borealis Formation, whose widespread nature provided us with a similar geological environment, similar "background" roughness characteristics (Kreslavsky and Head 2000), and, presumably, a uniform onset of crater population formation (Head et al. 2002; Tanaka et al. 2005). We excluded areas where dunes and other topographically pronounced features were present on the crater ejecta. We considered only craters with diameters D from 10 to 25 km. This narrow range of D assured the maximal possible similarity of the pristine ejecta pattern. Almost all these craters have double-layer ejecta (e.g., Barlow et al. 2000). For smaller craters, the ejecta are too poorly sampled with the Mars orbiter laser altimeter (MOLA). For larger craters, multiple-layer ejecta dominate (e.g., Barlow et al. 2000) and this ejecta morphology is different from the double-layer ejecta morphology of 10–25 km craters. We limited ourselves to high latitudes >52°N within the high-latitude "smoothed" zone (Kreslavsky and Head 2000). In total, 130 craters match these criteria. The craters are unevenly distributed because "typical" Vastitas Borealis material is not uniformly present through the northern lowlands.

Assuming an age of 3.1 Gyr for the Hesperian-Amazonian boundary (Hartmann and Neukum 2001) and hence the same onset for our crater population, one crater forms, on average, each 24 Myr. Obviously, only very approximate estimates of ages can be obtained from the counting of a small number of craters.

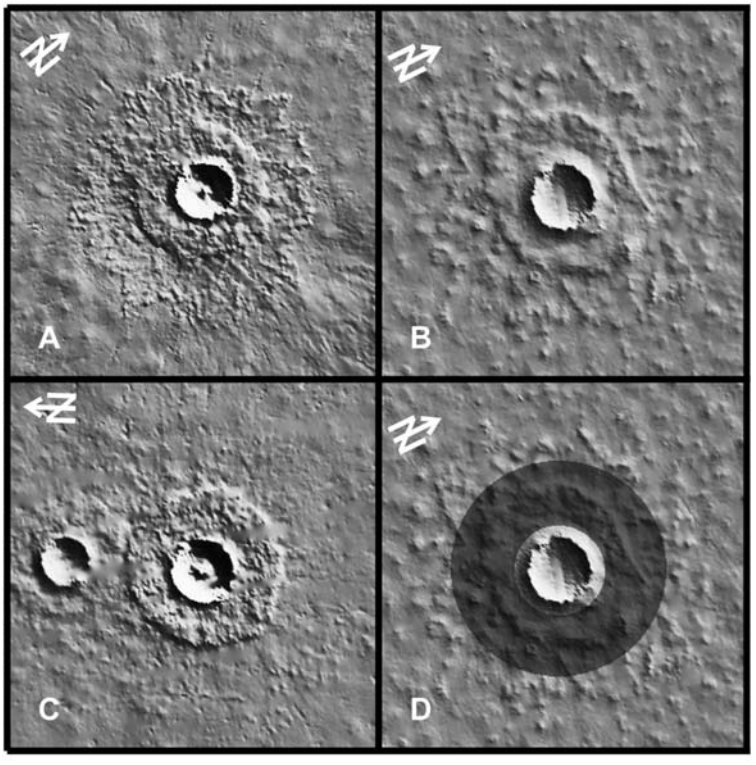

Fig. 2. MOLA-derived simulated shaded topography of three craters in the Vastitas Borealis Formation. a) "Fresh" crater A at 73.0°N, 38.3°E; crater diameter D = 12.0 km. b) "Altered" crater B at 73.0°N, 22.0°E; D = 12.9 km. c) The "second-roughest" crater C at 69.3°N, 274.0°E; D = 12.9 km. d) The area used for roughness statistics for crater B.

Morphometry

Diameter

We measured crater diameter D by fitting a circle to the crater rim crest as seen on 128 pixel/degree gridded topography derived from measurements of the MOLA (Smith et al. 2001) on board Mars Global Surveyor (MGS). This approach is sufficient for our analysis.

Wall Steepness

We used individual MOLA profiles to measure the steepness of the northern and southern crater walls. MOLA profiles are precise measurements of surface elevation with 0.3 km spacing along MGS orbits (Fig. 3). The orbit tracks have an approximately north-south orientation. Orbit passes are unevenly distributed, and the gaps between them can be as wide as a few kilometers. Our work with gridded topography has shown that it is not suitable for steepness measurements of the eastern and western walls of the craters. The elevation consistency between neighboring or crossing orbits is much worse than the high along-track precision of elevation differences, even after the crossover correction (Neumann et al. 2001). The reason for this is that the crossover correction adjusts the profiles vertically, while the errors in the MGS orbit determination also have horizontal components. For sharp slope breaks typical of crater walls, the vertical correction does not compensate the horizontal error. This effect is seen in the MOLA gridded topography as "disintegrated" eastern and western walls (this can be seen in Figs. 2a and 2b). Thus, we used the individual profiles and limited ourselves to the northern and southern walls.

For each crater, we selected all MOLA profiles that passed closer than 30% of the crater radius from its center, that is, those that crossed the crater close enough to its diameter. We excluded profiles that had missing data points on the crater walls. This selection criterion gave 1 to 19 (usually 4–12) good profiles for each crater. Tilts of the steepest segment of wall profiles were averaged over all profiles for a given wall, and this average was considered a measure of the wall steepness. All this processing was done in an automated manner. Cases of unusually steep or gentle profiles or unusually high scattering of wall steepness between profiles for the same wall were screened visually. On the basis of this screening, we excluded a few profiles where nighttime near-surface clouds (fogs) obviously distorted the measurements. Because MOLA passes are not exactly radial to the crater, they cross the crater walls at an angle, and the steepness of the profile in principle underestimates the tilt of the wall. However, we did not introduce any specific correction for this underestimation because it is small (less than a few degrees) and less than other variables (e.g., local variations in the wall shape).

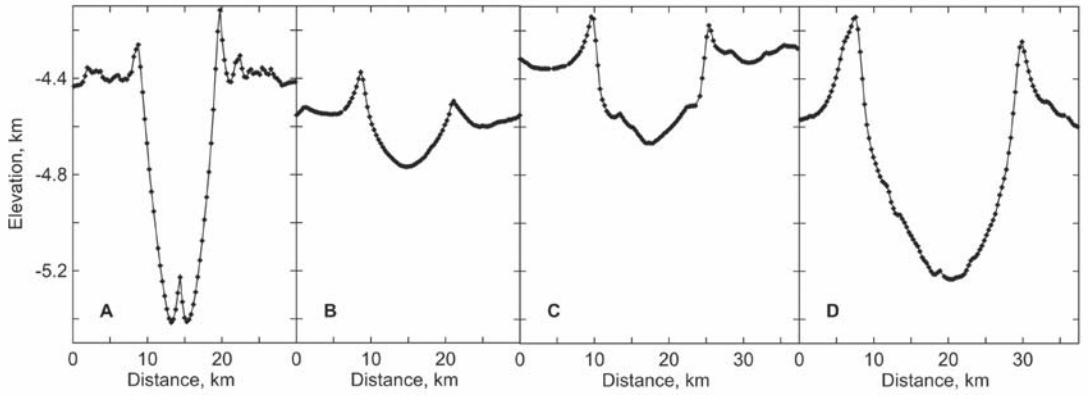

Fig. 3. Examples of MOLA profiles of craters. All profiles have the same scales; vertical exaggeration is 32 times. a) Crater A at 73.0°N, 38.3°E, the same as shown in Fig. 2a; MOLA pass 19296. The crater is deep and has steep walls and a central peak. b) Crater B at 73.0°N, 22.0°E, the same as shown in Fig. 2b; MOLA pass 19517. The crater is shallow and bowl-shaped, and has gently sloping walls. c) A crater at 60.4°N, 115.9°E (crater diameter D = 14.9 km); MOLA pass 20104. The crater is shallow, and has ~20° steep walls and a convex floor profile. d) A crater at 66.4°N, 163.5°E (crater diameter D = 22.0 km); MOLA pass 11634. An image of this crater is shown in Fig. 6. A pristine crater of such size is expected to be significantly deeper.

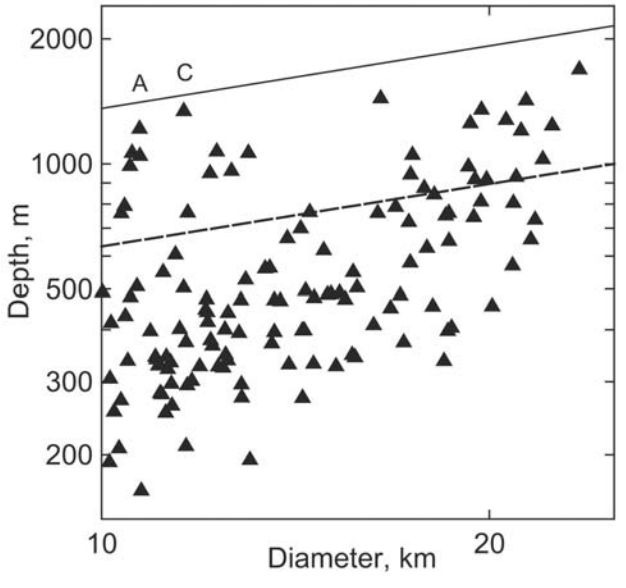

Fig. 4. Depth-diameter distribution of the crater population analyzed in this study. Both axes have logarithmic scales. The dashed line shows the global depth-diameter trend line from Garvin et al. (2001); the thin, solid line corresponds to normalized depth $d^* = 1$. Craters A and C are marked with letters.

The scattering displayed by the tilts of the steepest segments of MOLA profiles is of course high because the wall topography is intrinsically complex. Some craters in the survey are very shallow (200–300 m); for such craters, there may be steep wall segments that are narrow in comparison to the distance between measurements along the MOLA profiles, and the wall steepness may be underestimated locally.

The zone of very strong systematic north-south slope asymmetry (Kreslavsky and Head 2003), where pole-facing crater walls are much gentler than equator-facing ones, is located south of our survey area. We looked for systematic north-south asymmetry in wall steepness in our data set. Among craters with steep walls in the 60–70° latitude, there is a tendency for southern (pole-facing) walls to be steeper than northern (equator-facing) walls. This tendency is not well pronounced, and should not be considered established. We use an "average" wall steepness combining northern and southern walls for some illustrations below.

Depth

We measured crater depth d by averaging the peak elevations for the northern and southern walls from the profiles used for measurements of the wall steepness and in turn using this as a measure of rim elevation. The minimal elevation in the gridded topography inside the rim was taken as a measure of the floor elevation. The difference of these two was taken as a measure of crater depth.

The depth-diameter scattering diagram for the crater population studied is shown in Fig. 4. The wide range of crater depths in the northern plains has been noted in a number of studies (see Garvin et al. 2000; Boyce et al. 2005 and references therein) and is obvious in this figure. For our narrow diameter range, a specific correlation between depth and diameter is not seen. Figure 4 also shows the global depth-diameter trend inferred from the much wider diameter range analyzed by Garvin et al. (2000): $d = 190\ D^{0.55}$, where d is in meters and D is in kilometers. Depth d itself is not a good measure for the analysis of crater modification because larger pristine craters are deeper; the depth/diameter ratio d/D is not a good choice either because larger pristine craters have lower d/D. In our analysis, we use a normalized crater depth d^*, the crater depth with the global depth-diameter trend removed. We define this quantity as $d^* = d / (430\ D^{0.5})$, where d is in meters and D is in kilometers. The exponent 0.5 was chosen as close to that of the global depth-diameter trend; the

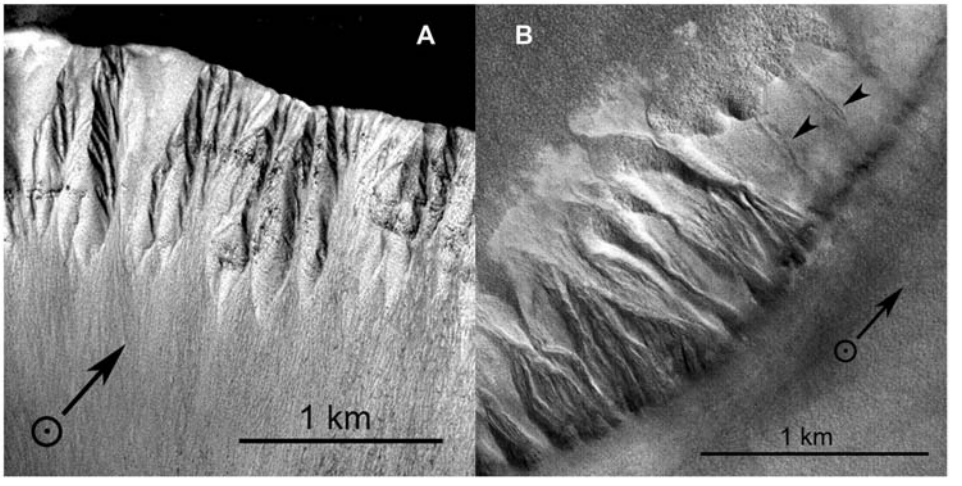

Fig. 5. a) Chutes on the northern wall of crater C (69.3°N, 274°E); a portion of MOC image E04/00537. Chutes erode the layered bedrock. b) Chutes on the southeastern wall of a crater at 58.2°N, 90°E; a portion of MOC image R04/02021. Chutes erode a thick mantle material on the crater wall. The short arrows show features that may be interpreted as old chutes or gullies covered by a mantle later emplaced. The long arrows show illumination direction.

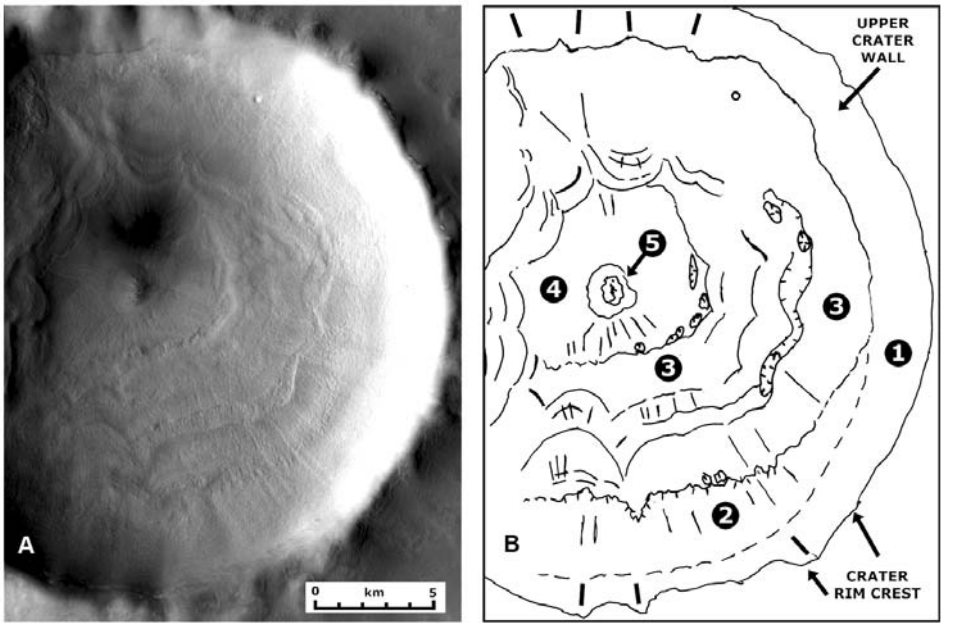

Fig. 6. A crater at 66.4°N, 163.5°E, diameter D = 22.0 km, normalized depth d^* = 0.52. The south-north profile of this crater is shown in Fig. 3d. a) A portion of THEMIS image V05250022. b) A scheme of the main morphological features and zones (see text). Tick marks indicate scarps.

factor 430 was arbitrarily chosen so that the maximal $d^* \sim 1$. The line $d^* = 1$ is also shown in Fig. 4.

Morphology

To study crater morphology, we used Mars Odyssey thermal emission imaging system visible-imaging subsystem (THEMIS VIS) images (Christensen et al. 2004) of ~20 and ~40 m/pixel resolution, and MGS Mars orbital camera narrow-angle (MOC NA) images (Malin and Edgett 2001) of ~1.5–12 m resolution. THEMIS VIS images usually include the entire crater or a significant part of it, which makes them useful for a general assessment of crater morphology. The quality of images is very different, depending on the presence of hazes and clouds, illumination conditions, season, and exposure settings. The presence of seasonal CO_2 frost in a number of images taken during northern spring and early summer strongly affects the appearance of crater morphology in the images. We encountered examples where fresh chutes on the crater walls were clearly seen in 20 m/pixel

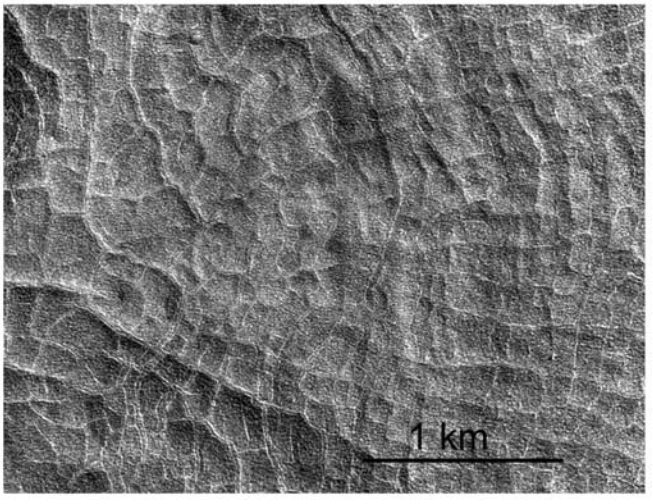

Fig. 7. The characteristic coarse polygons on a crater floor are superposed by small-scale polygonal pattern. Crater at 61.5°N, 21.8°E; a portion of MOC image E21/01593.

high-quality THEMIS images and were "clearly absent" from 40 m/pixel springtime images taken through a hazy atmosphere. MOC NA images show crater floor and wall morphology in high detail, but they never cover the entire crater. Among our 130 craters, 109 have one or more high-resolution images.

Figure 6 shows a crater, 22 km in diameter and 1.0 km deep ($d^* = 0.52$), that provides a good example of the interior morphology of the craters studied. Five generally concentric zones can be identified from the crater rim crest inward to the interior. In the outermost zone 1, just below the rim crest, slopes are relatively steep (Fig. 3d; ~20°). In zone 2, and seen particularly well at the southern part of the crater wall, the slope decreases (~5–10°), and the surface has linear features that are generally radial to the crater. Zone 3 consists of a series of arcuate, convex-inward, lobe-like features defined by a series of concentric ridges; lobes range from 2 to 5 km in width. Some of the ridges in the lobes appear to have been replaced by elongated pits and depressions, particularly on the eastern side of the crater interior. The boundary between zones 2 and 3 is characterized by an outward-facing sinuous scarp and occasional small pits. Zone 3 is sloping at ~1–5°. Its inner margin is defined by an inward-facing scarp consisting of multiple lobes. Zone 4 is characterized by a coarsely polygonal pattern, but radial troughs tend to dominate. Some circular-to-elongate pits are seen at the boundary between zones 3 and 4. The innermost zone, 5, consists of a remnant blocky central peak surrounded by talus slopes, standing above the local surrounding crater floor. Two scales of polygons are observed in the crater interior: 1) coarse polygons (50–250 m in diameter) cover zones 3 and 4 and their margins make up some of the radial and concentric patterns in the lobes and other zones; and 2) smaller polygons (the "basketball" texture, 10–40 m in diameter; better seen in MOC images) are superposed on the larger ones throughout the interior of the crater, as well as onto the walls and rim, but are absent in zone 2.

Coarse polygons similar to those in zones 3 and 4 (Fig. 6) are seen in 38 craters (see a high-resolution view in Fig. 7; see also MOC images E03/00299 for a spectacular high-resolution view). These polygons (type LT, according to Mangold 2005) have a very specific morphology and are distinctive from all other patterned ground widely distributed at high latitudes on Mars. Polygons with this morphology are observed only on crater floors and never outside craters. Twenty craters have no such polygons; we do not see such polygons in the remaining 51 craters, but the image coverage is not sufficient to be sure that they are absent.

Small polygons (types S2, S3, according to Mangold 2005) are typical of the high-latitude, ice-rich mantle (see Kostama et al. 2003; Kreslavsky and Head 2002a; Head et al. 2003) and are interpreted as sublimation polygons (Marchant and Head 2005). They are present almost everywhere, where resolvable in the MOC images, both in craters and in the "background" surface of the Vastitas Borealis Formation. Coarse polygons are covered with the small polygons (Fig. 7). Dissection patterns related to degradation of this mantle (e.g., Mustard et al. 2001; Head et al. 2003) are observed in the mantle material mostly in association with crater walls (Fig. 5b) or in the southern parts of the surveyed area (e.g., zone 2 and pits in zone 3) (Figs. 5b and 6).

Arcuate inside ridges, folds, and lobes (convex toward the crater center) more or less similar to those in zone 3 (Fig. 6) are observed in 66 craters in total. The morphology of these features varies from crater to crater.

Fifteen craters have what we refer to here as "chutes" on their walls (see examples in Fig. 5). Unlike the gullies described by Malin and Edgett (2000) and further analyzed by many authors, our chutes have no unambiguous indication of liquid flow; they also may result from dry mass wasting. However, their presence clearly indicates recent slope processes and the absence or disruption of the icy mantle by such processes. Forty-three craters clearly do not have chutes on their walls. For the remaining 51 craters, we do not see chutes; however, the coverage and/or quality of the images is not sufficient to be sure that they are absent. Within our small sample of 15 craters with chutes, we do not see any convincing latitudinal or regional trend in chute occurrence. Chutes are often concentrated on one of the crater walls, but in our small sample we do not see any convincing trend in orientation.

Dark dunes are found on the floors of 28 craters. There is a well-pronounced regional trend in the presence of the dark dunes: most of them are clustered in a wide region around large dune fields. Thus, almost all craters with dunes also have numerous dunes surrounding their exterior (craters with dunes on their ejecta were excluded from the survey). Two craters with a few tiny, dark dunes on their floors are far away from the large dune fields.

Ejecta Roughness

As a measure of ejecta roughness, we used the median total surface curvature, which we calculated in the following way. We took advantage of the high density of MOLA measurements at high latitudes and used gridded topographic data at a resolution of 128 pixels/degree. In each pixel we calculated a finite-difference approximation of the matrix of second derivatives using the shortest possible baseline (0.9 km). The eigen values of this matrix gave the pair of principal curvatures C_1 and C_2 of the surface at each point. We defined the "total" curvature as $C = (C_1^2 + C_2^2)^{1/2}$. For each of the 130 craters, we manually outlined the test ejecta area as a ring loosely inscribing the inner ejecta lobe and excluding the crater rim and floor (Fig. 2d). For clearly asymmetric ejecta, we drew a noncircular outline. We preferred this way to mark the test areas because it allowed us to exclude small craters that overlap the ejecta, as well as to treat overlapping ejecta carefully. For each of 130 test areas, we calculated the median total curvature and used it as a measure of roughness.

ANALYSIS

Ejecta Smoothing

As we described above, crater A (Fig. 2a) has a fresh-appearing ejecta pattern and thus can be considered a relatively young crater. Quantitative measurements of crater ejecta roughness show that its ejecta are the roughest among the entire population studied (Fig. 8). Only one crater, crater C, has ejecta roughness that is comparably high (Fig. 2c). Craters A and C are far from each other on the surface and are surrounded by craters with much smother ejecta; thus, their rough ejecta deposits are probably not a regional effect. All other craters in the population studied have much smoother ejecta (Fig. 8) similar to crater B (Fig. 2b); their roughness is similar to or a little higher than the typical roughness of the "background" surface of the Vastitas Borealis Formation (Fig. 8). We interpret craters A and C to be the youngest craters in the population. Remembering that one crater in the population studied forms every 24 Myr on average, the number of craters with rough ejecta (2) indicates that the ejecta smoothing process occurs on a time scale of tens to hundreds of Ma, which is very short in comparison to the duration of Amazonian epoch.

The observed ejecta smoothing is part of the global latitudinal trend of small-scale roughness (Kreslavsky and Head 2000). Visual inspection of the roughness maps show that crater ejecta smoothing does not occur outside the high-latitude zone of general subkilometer-scale smoothing. High-latitude smoothing is accompanied by high concavity of subkilometer-scale topography (Kreslavsky and Head 2002a). We previously concluded that this smoothness and high concavity are due to smooth fill of local topographic lows

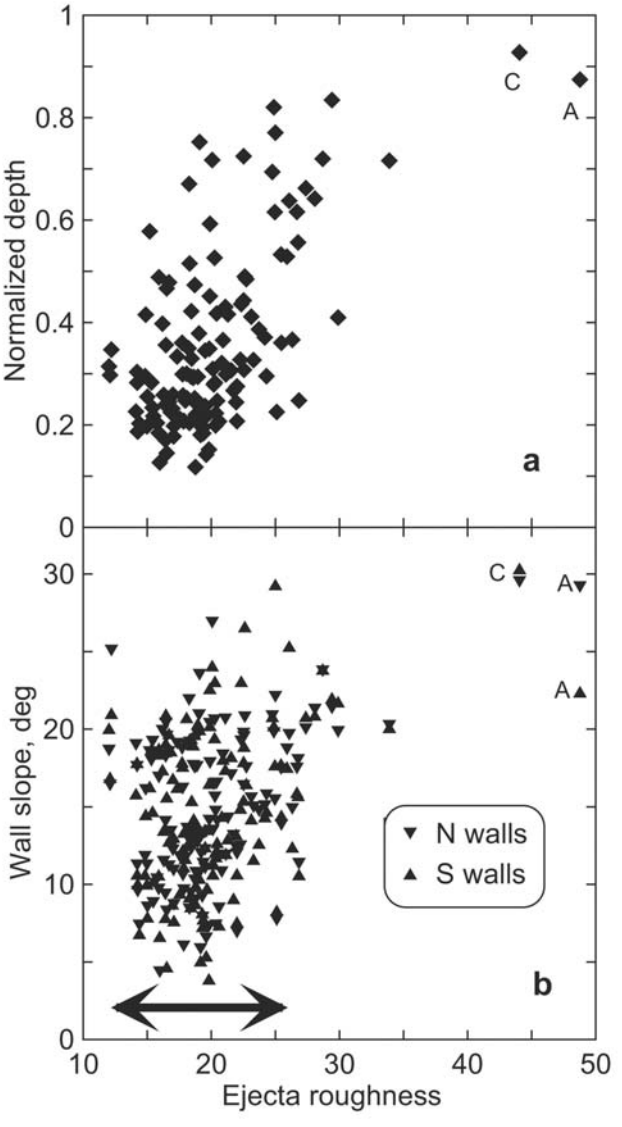

Fig. 8. Normalized depth (a) and wall slopes (b) of 130 craters plotted against ejecta roughness in arbitrary scaled units. Craters A and C have the roughest ejecta. Crater B is inside the dense clusters in the plots. The horizontal arrow shows the range of roughness of the typical Vastitas Borealis Formation surface outside the crater ejecta.

with icy mantle material (Kreslavsky and Head 2002a). The deposition of icy mantles at high latitudes was attributed to a global redistribution of H_2O ice on the planet, which was caused by climate changes driven by obliquity variations (Mustard et al. 2001; Head at al. 2003; Levrard et al. 2004).

High-resolution images of the ejecta of craters A (Fig. 9) and C (see MOC NA images M00/02273, M03/00960, and E04/00537) show the presence of the mantle superposed on their ejecta. The mantle is eroded around local sharp knobs revealing its layered structure; two to three layers are usually seen. This means that both of these youngest craters are older than a few of the most recent episodes of mantle emplacement and at least one episode of mantle ablation. This observation

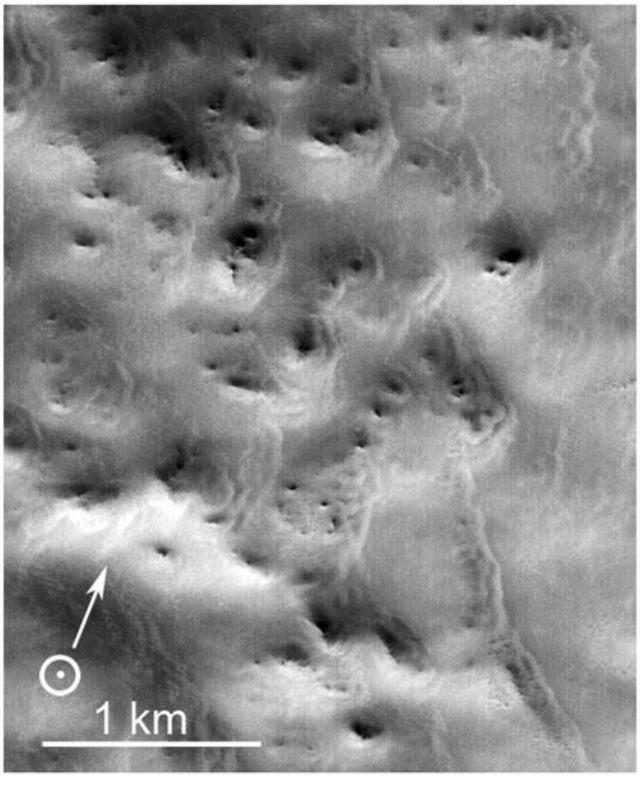

Fig. 9. Ejecta of crater A; a portion of MOC image E17/00562. The surface is covered with seasonal frost. The arrow shows the illumination direction.

also indicates that the high-latitude smoothing does not result from a single mantle layer but is a consequence of repeated cycles of mantle emplacement and ablation. At lower latitudes, where the mantle is partly dissected, it is often seen that the dissection begins at local highs, while the mantle is often preserved in local lows. On the basis of these observations, the smoothing mechanism is better understood: ablation is apparently less effective in local lows, and some mantle material in local lows survives the ablation episodes and contributes to the progressive fill of local lows. This may be due to shadowing of the lows and/or due to thicker dust residue in the lows inhibiting sublimation. Erosion of bedrocks at local highs during ablation episodes can also contribute to topography smoothing. We believe, however, that its role is minor, because even the oldest craters preserve the general topographic signature of two-layer ejecta, indicating that the total loss of ejecta material was not voluminous.

Several studies have shown that the ejecta volume of typical craters in the northern lowlands of Mars is noticeably greater than the cavity volume (e.g., Garvin et al. 2000; Black and Stuart 2005). This has been attributed to deflation of material surrounding the ejecta (an effect similar to pedestal crater formation), which increases the apparent ejecta volume, as well as to crater filling, which decreases the cavity volume. Our morphological observations indicate that emplacement of the mantle material in local lows contributes to an increase of apparent ejecta volume. As an example, we present rough volume estimations for the fresh crater A with single profile shown in Fig. 3a and Fig. 13 (bold lines). The volume of the inner ejecta lobe plus rim is 60% of the cavity volume (the topography of the outer ejecta lobe is not pronounced enough to estimate its volume with MOLA data). If we fill lows in the inner ejecta as shown in Fig. 13c with a dashed line, this would add 50% of the cavity volume, and thus the total apparent ejecta volume would exceed the cavity volume.

Wall Erosion

The steepest crater walls in the population studied have slopes of about 30°; the majority of craters have more gently sloping walls (Figs. 10a, 8b, and 12). The global statistics of steep slope occurrences on Mars (Kreslavsky and Head 2003) have shown that both north and south high-latitude regions are devoid of steep slopes. Slopes steeper than 30° are typical for craters in the equatorial regions. Figure 12 compares wall steepness (and depth) for the population studied (solid symbols) with all 32 craters in the same diameter range in Lunae Planum composed of homogeneous Hesperian-age volcanic plains at low latitudes (empty symbols). All crater walls in Lunae Planum (except one) are steeper than 20°, while the slope of the majority of the walls in our population is gentler, despite the whole population being somewhat younger. The lack of steep slopes does not result from any specific characteristics of the Vastitas Borealis Formation material, because a similar global trend also occurs in the southern hemisphere, where the Vastitas Borealis Formation is absent; this is certainly the result of wall alteration, and this alteration is climate-controlled because it has a distinctive latitudinal occurrence.

The youngest craters, A and C, have walls that are among the steepest in the population studied (Fig. 8b); this supports the conclusion that slopes experience degradation with age. These craters, however, are not the only craters with steep walls. The steepness frequency distribution is shown in Fig. 10a. The distribution has a sharp step at about 20° slope. Such a distribution cannot be explained by any process that operates on all slopes continuously throughout the Amazonian. As an illustration, a model distribution for the case with slope degradation rate proportional to slope steepness is shown in Fig. 10a. The distribution step at 20° slope can be interpreted in two alternative ways. 1) One possibility is that some effective erosion process has been active (continuously or episodically) during some recent periods, but did not operate prior to that time. The number of craters with walls steeper than 20° (12) provides an estimate of 210–430 Myr for the duration of this active wall degradation period (90% confidence level). If this is the case,

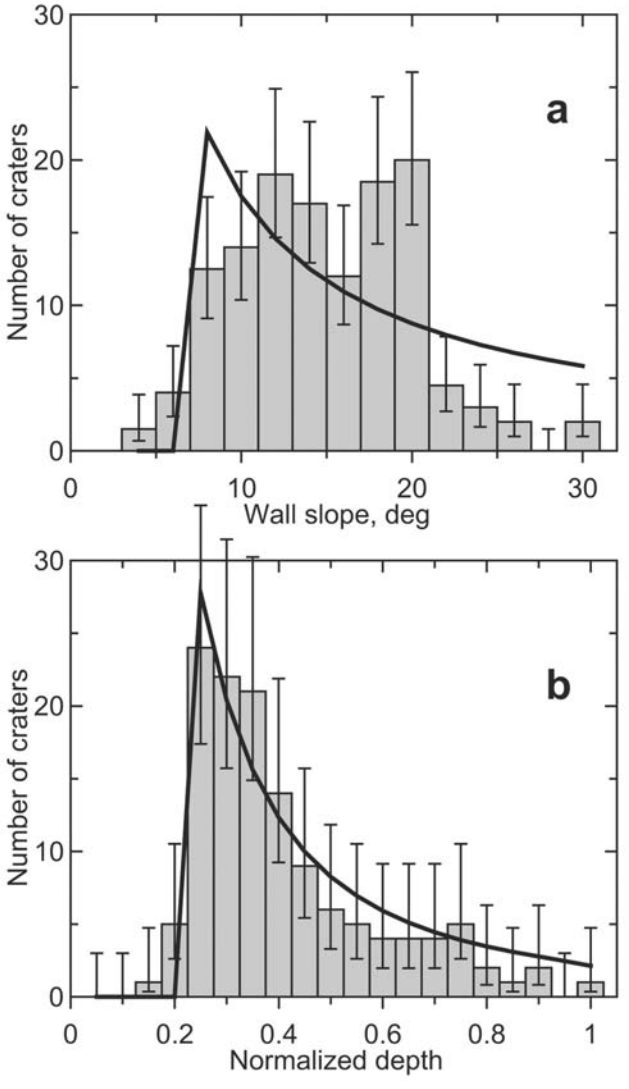

Fig. 10. The incremental frequency distribution (bars) of wall slopes (a) and normalized depth (b). Error bars show formal 95% confidence interval for frequency expectation in each bin. Curves show model frequency distributions: (a) the wall-degradation rate is proportional to the slope tangent; (b) the crater-filling rate is proportional to the square of the depth.

this implies strong climate change in the Late Amazonian period. 2) A second possibility is that some active slope-degradation process has a very sharp onset at 20° slope and operated throughout the entire Amazonian epoch.

The morphology of the walls clearly indicates that wall-erosion processes that form chutes (Fig. 5) are responsible for, or at least contribute to, slope degradation. Downslope movement of material by chute-forming processes increases small-scale slopes at the chute walls and decreases the larger-scale slopes of the crater walls. The nature of the chute-forming process is unclear. The whole list of processes proposed for formation of gullies, including flowing water, wet debris flow, flow of dry material, density flow, flow of

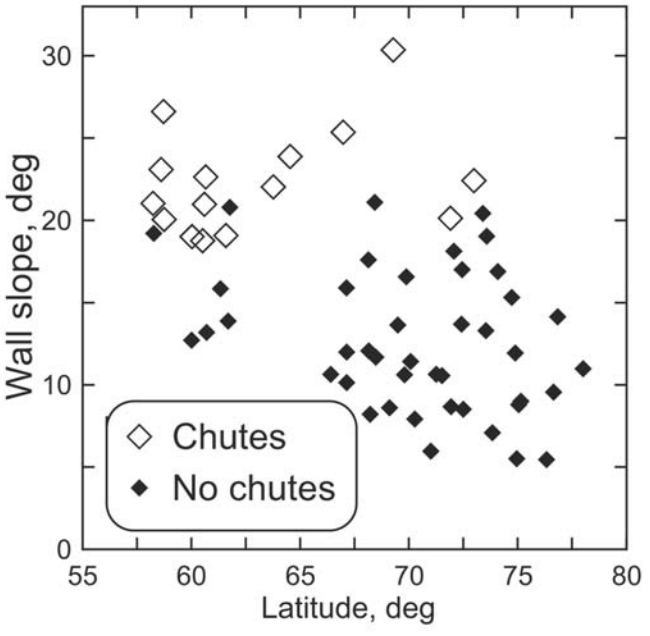

Fig. 11. Wall slope (average of the northern and southern walls) plotted against latitude for craters with and definitely without chutes on crater walls.

liquid CO_2 (for a recent review see Heldmann et al. 2005) can often be applied to chutes even better than for gullies. Figure 11 shows the latitudes and wall slopes for craters with and certainly without chutes. The occurrence of chutes does not depend on latitude in the latitude range of this study; it is, however, correlated with slopes. All craters with steep walls (>21°) have chutes, and there are no chutes in craters with gentle walls (<18°). Thus, we see that the chute formation process has a sharp onset at ~20° slope, which coincides remarkably with the step in the slope-frequency distribution (Fig. 10a). This coincidence of the chute onset and the step in the slope-frequency distribution tends to support scenario (2) above. It is not clear, however, what downslope movement process can have a sharp onset at 20° slope. Dry mass movement usually has an onset close to the angle of repose, that is, noticeably steeper than 20°. Cryoturbation and fluid flows do not have an onset angle; for wet debris flows, it is not clear how the onset can be that sharp. Thus, we do not see enough evidence to completely reject scenario (1). In any scenario, the generally flat distribution in the 10–20° slope interval indicates a very slow degradation of crater walls, on average, with such slopes through most of the Amazonian era.

Crater Fill

The depth/diameter ratio of craters in the northern lowlands is known to be scattered over a very wide range; this scatter has been explained by crater-modification processes (e.g., Garvin et al. 2000; Boyce at al. 2005). In our survey, the youngest craters, A and C, are among the deepest and have the

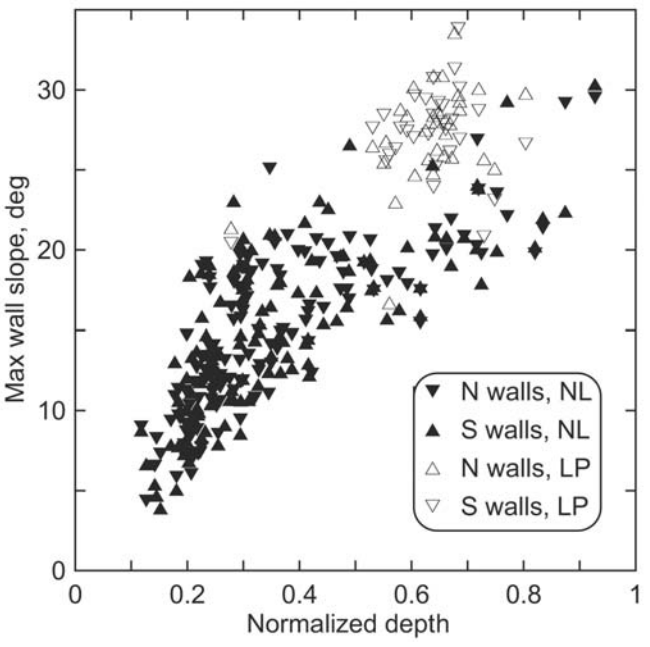

Fig. 12. Wall slope plotted against normalized depth for all craters in the survey (NL, solid symbols) and for craters in Lunae Planum (LP, open symbols). Morphometric characteristics of all craters 10–25 km in diameter in Lunae Planum were measured in the same manner, as in the northern lowland survey.

highest normalized depth d^* among the entire population (Fig. 8a). There is some correlation between normalized depth and wall slopes (Fig. 12; the correlation coefficient between d^* and tangent of wall slope is 0.76). All these observations confirm that the decrease of crater depth occurs in the context of aging of the craters. Data about similar craters in Luane Planum (Fig. 12) show that for the equatorial region there is no such decrease: all craters (except one) are deep ($d^* > 0.5$), and there is no correlation with wall steepness. Note that the deepest craters in the northern lowlands are even deeper than in Lunae Planum (Fig. 12), which again indicates that the shallowness of the northern lowland craters is the result of alteration rather than peculiarity of emplacement.

The normalized depth-frequency distribution (Fig. 10b) is well approximated by a model of accumulation crater population, in which at time of origin $d^* = 1$, the oldest crater has $d^* = 0.2$, and the rate of the decrease of d^* is proportional to the square of d^*. Thus, the distribution indicates that shallowing is much more effective for deep craters than for shallow craters. The characteristic time scale of this process is comparable to the duration of the Amazonian.

We do not believe that gravitational relaxation of craters plays a role in crater shallowing. Large features with high topographic amplitudes have been preserved on Mars since the Noachian, indicating a strong lithosphere in the post-Noachian period (e.g., Solomon et al. 2005); quantitative geophysical analysis for the northern lowlands (Johnson et al. 2000) led to the same result. We modeled gravitational relaxation of a crater semianalytically following Ramberg (1981). This simple linear method assumes Newtonian rheology and is not suitable for detailed quantitative modeling, but allows rapid first-order understanding of the main features of the relaxation process and is totally independent of any assumptions about material properties. We adapted the method for calculations in cylindrical coordinates and used one of the radial profiles of crater A for the initial surface topography. Figure 13b shows a sequence of profiles for a semi-infinite plastic medium. It is seen that the relaxation process preserves the central peak of the crater. Several deep craters in our population have central peaks (including craters A and C), but among the shallowest one-third of the population, central peaks are not observed.

Some workers have suggested that the northern lowlands are covered with deposits a few km in thickness containing a considerable amount of ice (e.g., Clifford 1993; Clifford and Parker 2001) and hence mechanically weak. Gravitational relaxation of a crater in a plastic layer over a rigid surface reduces the height of the central peak (Fig. 13c); however, it also inevitably leads to depression of the crater rim, which is not observed. On the basis of these considerations, we conclude that gravitational relaxation plays no role in crater shallowing, and that craters become shallower with time due solely to filling with additional material.

Simple mass wasting of material from the crater walls is not completely responsible for crater filling. Mass wasting would remove crater rim crests and rims; however, all Amazonian craters in the northern lowlands have well-preserved rims. Figure 13a shows the model result for crater modification by diffusion creep (e.g., Perron et al. 2003), a process in which the downslope mass-movement rate is proportional to slope steepness. It is seen that the rim disappears much earlier than the cavity becomes noticeably shallower. Nonlinear mass wasting would preserve the slope break at the top of the crater wall, but it would remove the rim even more effectively. Estimates of rim volume for fresh craters A and C are scattered within 5–25% of the cavity volume for different radial profiles; since the rims are preserved in the older craters, the wall erosion contribution to the crater fill is a few percents or even smaller. Thus, we conclude that filling material comes largely from outside of the crater.

As we noted above, craters located in the general vicinity of sand dune fields have dark dunes on their floors. Migrating sands are trapped within craters with steep walls. This is obviously one of the mechanisms that contribute to crater filling. As we observed, sand trapping has a regional occurrence, depending on the availability of sand in the recent past. This indicates that the crater-fill rate can vary regionally. This is why it is not surprising that the correlation between crater depth and wall steepness (Fig. 12) is not high.

Migrating sand is not the only contributor to crater

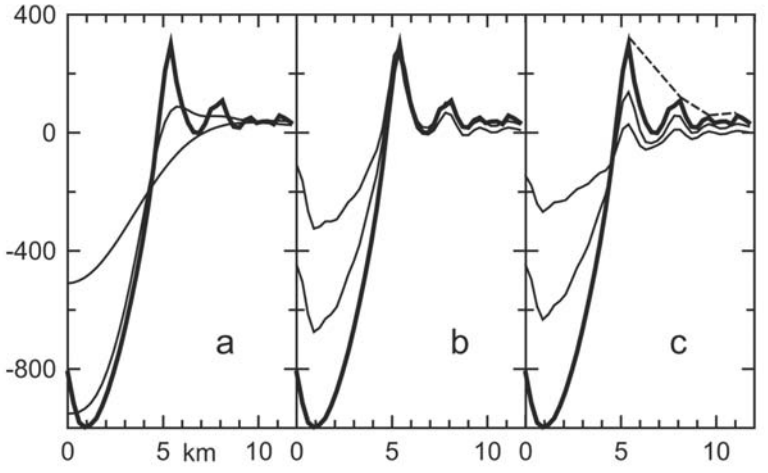

Fig. 13. Simple linear models of crater shallowing: a) diffusion creep, b) gravitational relaxation in a plastic halfspace, and c) gravitational relaxation in a plastic layer 2.5 km in thickness. The radial profile of crater A (one-half of the profile shown in Fig. 3a) was taken as the initial topography (bold line). The two thin lines show the calculated model radial profiles for two ages; the difference between ages is 10 times for (a) and 3 times for (b) and (c). The dashed line in (c) shows simulated smoothing of ejecta by mantle emplacement.

filling, because floors of the majority of the craters are covered by material of another kind. A coarse polygonal pattern (Fig. 7) typical of crater floors indicates the presence of ice in this material. Figure 14 shows latitudes and normalized depth d^* for craters with and certainly without such polygons. Within our high-latitude zone, the polygon occurrence does not depend on latitude. However, there is a well-pronounced relation to crater depth: polygons are never present in deep craters. Thus, the polygons are formed only if the filling material is thick enough. Polygons of this kind have not been found outside craters (Mangold 2005). The thermal regime of the crater floors does not differ significantly from the surroundings, and therefore the presence of the specific polygons is more likely to be due to the specific material of the crater fill. This material is either completely absent outside the craters or is present in thin layers not capable of forming polygons with such a large size.

Concentric or arcuate convex inward ridges or folds (Fig. 6) indicate plastic deformation of the filling material with modest strain. The floors of partly filled craters often have convex topographic profiles (Fig. 3c) with a depression in the floor center. Mass-wasting processes produce concave profiles; the convex topography unequivocally indicates plastic deformation of a thick layer. Craters with convex profiles usually also have arcuate convex-inside ridges or lobes, which are also suggestive of flow. The plastic behavior of the filling material is also suggestive of a high ice content for this material.

On the basis of the details of crater-interior morphology (Fig. 6), we infer that the icy interior deposits evolved when, at some time in the past, thick (on the order of hundreds of meters) deposits of ice were formed on the lower parts and the base of the crater walls (their origin is discussed below). Downwasted debris from the walls added a minor non-ice

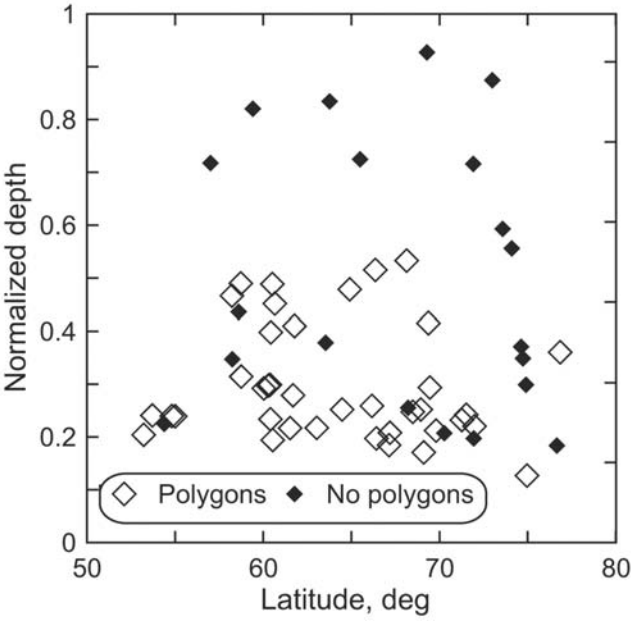

Fig. 14. Normalized crater depth plotted against latitude for craters with and definitely without coarse polygons on the floors.

contribution to this material. Slow downslope flow of this material produced unique convex topographic profiles, and created arcuate fold structures like those in zone 3 (Fig. 6); flowing material filled the crater floor, banking up against the central peaks, and covering and obliterating them with time. Sublimation removed ice from uppermost layers of the material; the sublimation till preserved the main body of the deposits from further sublimation. Continued climate-related thermal cycling formed the coarse polygons in the interior (zones 3–4, Fig. 6). Elongate troughs and pits were formed by sublimation of enclosed ice, particularly where folds had

thinned the debris cover. The local thermal regime at the base of the walls favored sublimation and removal of the fill material; this is responsible for absence of the coarse polygons in zone 2 (Fig. 6), for the outward-facing scarp at the boundary between zones 2 and 3, and for scarps in Fig. 5b. Late-stage climate-related mantles form and evolve, producing the "basketball" pattern of the sublimation polygons.

The origin of the ice that evolves in the described way is not certain. Successful hypotheses should not only propose its presence in craters, but also the absence of deposits outside. We consider a number of such hypotheses.

1. *Glacier-like scenarios.* Under certain climate conditions in the past, a crater's walls, wall base, or floor can be the preferred location for frost and/or snow accumulation due to specific microenvironments, insolation patterns, transient perennial CO_2 deposits after low-obliquity periods (Kreslavsky and Head 2005), etc. Insolation-related factors favorable for ice accumulation operate differently on the northern and southern walls of the craters. We carefully analyzed the topographic profiles of the crater floors looking for north-south asymmetry. Floor topography of partly filled craters is often very complex; sometimes the floor is inclined and/or has a very asymmetric profile. We failed, however, to find any consistent pattern in this asymmetry. Local conditions favorable for ice accumulation may not be related to insolation. For example, walls can trap wind-blown snow in wind shadows. Alternatively, numerous "ice ages" with deposition and subsequent removal of thin ice mantles may cause long-time-scale accumulation of ice at the crater wall base due to ice downwasting and preferential protective covering with debris from the walls.
2. *Flood.* The filling material may be a residue of Amazonian-aged floods. A few outflow channels that empty into the northern lowlands show clear evidence for Amazonian age outflow events (see, e.g., Carr 1996 for a review). The volume of fluid delivered by these events to the northern lowlands, presumably liquid water, was significant. The estimated lower boundary of the water volume that passed through the channels during individual outflow events is less than the amount of water necessary to completely flood the lowlands, but the actual volume could easily be a factor of a few larger than the estimated lower boundary. Models show that the flood water quickly freezes and then sublimates (Kreslavsky and Head 2002b). Since the flood water column in the craters is an order of magnitude deeper than in the surrounding plains, it is quite probable that any ice resulting from a flood completely or almost completely sublimated from the plains, but a significant part could be preserved in craters. Furthermore, it is probable that the ice near the crater walls would be preferentially covered by mass-wasted debris and protected from sublimation, while in the crater centers sublimation could continue. If this hypothesis is true, we should expect a pronounced morphological difference between craters that predate and postdate the most recent flood. Thus far, however, we do not observe any striking morphological differences of this kind.
3. *Deep groundwater.* The filling material could be from an underground source. The presence of an overpressurized aquifer below a cryosphere a few kilometers in thickness in the northern lowlands was hypothesized by Clifford (1993) and Clifford and Parker (2001), and the possible role of underground water for the Vastitas Borealis Formation was discussed by Tanaka et al. (2003). Leaking of water from such an aquifer could produce the distinctive icy material in the crater interiors. So far, however, we do not see any positive evidence for an underground source for the filling material; we also have no observations that would clearly reject it. A specific search (Russell and Head 2002) showed no traces of groundwater in the largest crater in the northern lowlands. If partial filling of craters with groundwater occurred, it should have taken place over a short time (thousands of years) immediately after crater formation, while the thermal effect of the impact was in effect. If water failed to penetrate through the freshly disrupted and heated cryosphere, it is improbable that this would happen after the thermal effect of the impact dissipated. In such a scenario, after the crater is (partly) filled, the filling material would continue to evolve, as discussed for the flood hypothesis above. The degree of filling within this scenario does not reflect the crater age; it is defined by the conditions of the aquifer at the time of the impact. The absence of fill in the youngest craters could be interpreted to mean the absence of aquifer overpressurization during the present epoch.
4. *Shallow groundwater.* Sapping of water from shallow aquifers has been proposed as a cause of gully formation (Heldmann et al. 2005 and references therein). If this process occurred, it could lead to accumulation of ice at the crater-wall base. We do not believe, however, that shallow aquifers were common in the Amazonian. Thermophysical calculations of Heldmann et al. (2005) were based on the assumption that the thermal conductivity of the upper tens of meters of the surface is the same as that of the upper centimeter. This assumption is definitely invalid for high latitudes, where the material in the upper meters is known to contain much ice.

Flood and deep groundwater hypotheses consider crater fill as a phenomenon specific to the northern lowlands. Hypothesis (1) predicts similar crater fill in the southern hemisphere area. Detailed study of the craters and other features in the southern circumpolar area should permit testing of these hypotheses and the rejection of some.

DISCUSSION

Formation of the geologically young high-latitude icy mantle is responsible for ejecta smoothing. Head et al. (2003) suggested that the mantle was formed during the periods of high-amplitude obliquity oscillations 0.3–2.1 Myr ago and prior to 2.7 Myr ago (Fig. 1). Levrard et al. (2004) have argued that the mantle was formed as a result of the general transition from obliquity oscillations about 35° to oscillations about 25°; this transition occurred from ~5 to ~3 Myr ago. In any case, mantle formation is certainly related to increased obliquity in comparison to the present. It is very probable that all craters in the population including craters A and C, the two youngest, are older than 5 Myr, and it is almost certain that at least one of them is older than 5 Myr. This means that at least one of the craters A and C, and probably both, have experienced 1) high obliquity peaks (>40°), 2) the general transition to lower obliquity, 3) recent obliquity oscillations, as well as 4) mantle formation during some phases of this evolution. This is in agreement with the observed mantle layers on the ejecta of these craters. Other (older) craters in the population have smoother ejecta. This means that the smoothing episodes, presumably mantle formation, occurred several times between the youngest crater with smooth ejecta and craters A and C. Depending on the details of the mantle formation, this means either moderate mean obliquity or repeated transitions from generally higher to moderate obliquity. In any case, permanently low obliquity (the mean obliquity <20°, the peak obliquity <30°) can be excluded, because in this case no H_2O migration can occur. A permanently high obliquity is also not plausible, because at permanently high obliquity H_2O would migrate to equatorial regions and reside there. The time frame for this conclusion is from the end of predictive calculations of obliquity evolution (~10 Myr ago) to the probable age of the third youngest crater in the population, which is, with 90% formal confidence, 40–160 Myr old.

The slope-frequency distribution of the crater walls (Fig. 10a; see the "Wall Erosion" section) contains further constraints on obliquity history. On the basis of the global statistical characteristics of steep-slope distribution on Mars, we have concluded that steep slopes at high latitudes are removed due to the formation of an active layer, that is, by yearly thawing and refreezing of a layer centimeters in thickness of permafrost (Kreslavsky and Head 2003). This can occur only at very high obliquities, >40–45°. Depending on the ambient conditions and ground-ice abundance, the following active layer processes can contribute to slope removal: 1) segregation of meltwater and slope erosion by streams; 2) erosion by wet debris flows, the mechanism proposed by Costard et al. (2002) to explain recent gullies at lower latitudes; 3) solifluction, downslope movement of wet material over frozen substrate; 4) cryoturbation, a mechanism responsible for slope degradation according to Perron et al. (2003); 5) cryoclastic erosion, disintegration of rocks by water freezing in cracks. Among these mechanisms, only wet debris flows may have a slope threshold. However, it seems improbable that such a threshold is very sharp and the same for all slopes with accuracy of 2–3°, especially taking into account the wide morphological diversity of chutes. Hence, the statistically significant step in the slope-frequency distribution (Fig. 10a) probably cannot be explained by the dependence of wall-degradation rate on slope and should be explained through variations of the rate with time. The step requires a sharp change of the slope degradation rate at some epoch between 210 and 430 Myr ago. Before this time, the average slope degradation rate was much slower than during the Late Amazonian. We speculate that this means that the high obliquity peaks were absent or almost absent during a geologically long period prior to 210–430 Myr ago. Further studies of slope morphology and ice-related features in high- and mid-latitude regions on Mars should challenge this tentative conclusion.

Acknowledgments–We are thankful to an anonymous reviewer for numerous comments that helped to improve the manuscript. We gratefully acknowledge the use of Mars Orbiter Camera images readily available from Malin Space Science Systems at http://www.msss.com/moc_gallery and the use of THEMIS images readily available from Arizona State University at http://themis-data.asu.edu. The work was partly supported by NASA grant NAG5-12286.

Editorial Handling—Dr. Nadine Barlow

REFERENCES

Barlow N. G., Boyce J. M., Costard F. M., Craddock R. A., Garvin J. B., Sakimoto S. E. H., Kuzmin R. O., Roddy D. J., and Soderblom L. A. 2000. Standardizing the nomenclature of Martian impact crater ejecta morphologies. *Journal of Geophysical Research* 105:26,733–26,738.

Black B. A. and Stewart S. T. 2005. Impact crater geometries provide evidence for ice-rich layers at low latitudes on Mars (abstract #3044). Workshop on the Role of Volatiles and Atmospheres on Martian Impact Craters. CD-ROM.

Boyce J. M., Mouginis-Mark P., and Garbeil H. 2005. Ancient oceans in the northern lowlands of Mars: Evidence from impact crater depth/diameter relationships. *Journal of Geophysical Research* 110, doi:10.1029/2004JE002328.

Carr M. H. 1996. *Water on Mars.* New York: Oxford University Press. 229 p.

Costard F., Forget F., Mangold N., and Peulvast L.-P. 2002. Formation of recent Martian debris flows by melting of near-surface ground ice at high obliquity. *Science* 295:110–113.

Christensen P. R., Jakosky B. M., Kieffer H. H., Malin M. C., McSween H. Y., Jr., Nealson K., Mehall G. L., Silverman S. H., Ferry S., Caplinger M., and Ravine M. 2004. The Thermal Emission Imaging System (THEMIS) for the Mars 2001 Odyssey mission. *Space Science Reviews* 110: 85–130.

Clifford S. M. 1993. A model for the hydrologic and climatic

behavior of water on Mars. *Journal of Geophysical Research* 98: 10,973–11,016.
Clifford S. M. and Parker T. J. 2001. The evolution of the Martian hydrosphere: Implications for the fate of a primordial ocean and the current state of the northern plains. *Icarus* 154:40–79.
Garvin J. B., Sakimoto S. E. H., Frawley J. J., and Schnetzler C. 2000. North polar region craterforms on Mars: Geometric characteristics from the Mars Orbiter Laser Altimeter. *Icarus* 144:329–352.
Hartmann W. K. and Neukum G. 2001. Cratering chronology and the evolution of Mars. *Space Science Reviews* 96:165–194.
Head J. W., Kreslavsky M. A., and Pratt S. 2002. Northern lowlands of Mars: Evidence for widespread volcanic flooding and tectonic deformation in the Hesperian period. *Journal of Geophysical Research* 107, doi:10.1029/2000JE001445.
Head J. W., Mustard J. F., Kreslavsky M. A., Milliken R. E., and Marchant D. R. 2003. Recent ice ages on Mars. *Nature* 426:797–802.
Head J. W., Neukum G., Jaumann R., Hiesinger H., Hauber E., Carr M., Masson P., Foing B., Hoffmann H., Kreslavsky M., Werner S., Milkovich S., van Gasselt S., and The HRSC Co-Investigator Team. 2005. Tropical- to mid-latitude snow and ice accumulation, flow, and glaciation on Mars. *Nature* 434:346–351.
Heldmann J. L., Toon O. B., Pollard W. H., Mellon M. T., Pitlick J., McKay C. P., and Andersen D. T. 2005. Formation of Martian gullies by the action of liquid water flowing under current Martian environmental conditions. *Journal of Geophysical Research* 110, doi:10.1029/2004JE002261.
Johnson C. L., Solomon S. C., Head J. W., Phillips R. J., Smith D. E., and Zuber M. T. 2000. Lithospheric loading by the northern polar cap on Mars. *Icarus* 134:313–328.
Kieffer H. H. and Zent A. P. 1992. Quasi-periodic climate change on Mars. In *Mars,* edited by Kieffer H. H., Jakosky B. M., Snyder C., and Matthews M. S. Tucson, Arizona: The University of Arizona Press. pp. 1180–1233.
Kostama V.-P., Kreslavsky M. A., and Head J. W. 2003. Morphology of the high-latitude mantle in northern plains on Mars (abstract #3011). The Sixth International Conference on Mars. CD-ROM.
Kreslavsky M. A. and Head J. W. 2000. Kilometer-scale roughness of Mars' surface: Results from MOLA data analysis. *Journal of Geophysical Research* 105:26,695–26,712.
Kreslavsky M. A. and Head J. W. 2002a. Mars: Nature and evolution of young latitude-dependent water-ice-rich mantle. *Geophysical Research Letters* 29, doi:10.1029/2002GL015392.
Kreslavsky M. A. and Head J. W. 2002b. Fate of outflow channel effluents in the northern lowlands of Mars: The Vastitas Borealis Formation as a sublimation residue from frozen ponded bodies of water. *Journal of Geophysical Research* 107, doi:10.1029/2001JE001831.
Kreslavsky M. A. and Head J. W. 2003. North-south topographic slope asymmetry on Mars: Evidence for insolation-related erosion at high obliquity. *Geophysical Research Letters* 30, doi:10.1029/2003GL017795.
Kreslavsky M. A. and Head J. W. 2005. Mars at very low obliquity: Atmospheric collapse and the fate of volatiles. *Geophysical Research Letters* 32, doi:10.1029/2005GL022645.
Laskar J. and Robutel P. 1993. The chaotic obliquity of the planets. *Nature* 362:608–612.
Laskar J., Gastineau M., Joutel F., Robutel P., Levrard B., and Correia A. 2004. Long-term evolution and chaotic diffusion of the insolation quantities of Mars. *Icarus* 170:343–364.
Levrard B., Forget F., Montmessin F., and Laskar J. 2004. Recent ice-rich deposits formed at high latitudes on Mars by sublimation of unstable equatorial ice during low obliquity. *Nature* 431:1072–1075.
Malin M. C. and Edgett K. S. 2000. Evidence for recent groundwater seepage and surface runoff on Mars. *Science* 288:2330–2335.
Malin M. C. and Edgett K. S. 2001. Mars Global Surveyor Mars Orbiter Camera: Interplanetary cruise through primary mission. *Journal of Geophysical Research* 106:23,429–23,570.
Mangold N. 2005. High-latitude patterned grounds on Mars: Classification, distribution and climatic control. *Icarus* 174:336–359.
Marchant D. R. and Head J. W. 2005. Equilibrium landforms in the Dry Valleys of Antarctica: Implications for landscape evolution and climate change on Mars (abstract #1421). 36th Lunar and Planetary Science Conference. CD-ROM.
Mustard J. F., Cooper C. D., and Rifkin M. K. 2001. Evidence for recent climate change on Mars from the identification of youthful near-surface ground ice. *Nature* 412:411–414.
Neumann G. A., Rowlands D. D., Lemoine F. G., Smith D. E., and Zuber M. T. 2001. Crossover analysis of Mars Orbiter Laser Altimeter data. *Journal of Geophysical Research* 106:23,753–23,768.
Perron J. T., Dietrich W. E., Howard A. D., McKean J. A., and Pettinga J. R. 2003. Ice-driven creep on Martian debris slopes. *Geophysical Research Letters* 30, doi: 10.1029/ 2003GL017603.
Ramberg H. 1981. *Gravity, deformation and the earth's crust in theory, experiments, and geological application.* London: Academic Press. 452 p.
Russell P. and Head J. W. 2002. The Martian hydrosphere/cryosphere system: Implications of the absence of hydrologic activity at Lyot crater (abstract #1688). 33rd Lunar and Planetary Science Conference. CD-ROM.
Smith D. E. et al. 2001. Mars Orbiter Laser Altimeter: Experiment summary after the first year of global mapping of Mars. *Journal of Geophysical Research* 106:23,689–23,722.
Solomon S. C. et al. 2005. New perspectives of ancient Mars. *Science* 307:1214–1220.
Tanaka K. L., Skinner J. A., Hare T. M., Joyal T., and Wenker A. 2003. Resurfacing history of the northern plains of Mars based on geologic mapping of Mars Global Surveyor data. *Journal of Geophysical Research* 108, doi:10.1029/2002JE001908.
Tanaka K. L., Skinner J. A., Jr., and Barlow N. G. 2005. The crater production function for Mars: A –2 cumulative power-law slope for pristine craters >5 km in diameter based on crater distributions for northern plains materials (abstract #2162). 36th Lunar and Planetary Science Conference. CD-ROM.